**Biogeosciences
Discussions**

Simultaneous quantification of in situ infaunal activity and pore-water metal concentrations: establishment of benthic ecosystem process-function relations

L. R. Teal[1,2,*], E. R. Parker[2], and M. Solan[1,]**

[1]Oceanlab, University of Aberdeen, Newburgh, UK
[2]Centre for Fisheries and Aquaculture Science (CEFAS), Lowestoft, UK
[*]now at: IMARES, Haringkade 1, 1976 CP Ijmuiden, The Netherlands
[**]now at: Ocean and Earth Science, National Oceanography Centre, University of Southampton, Waterfront Campus, European Way, Southampton, SO14 3ZH, UK

Correspondence to: L. R. Teal (lorna.teal@wur.nl)

8541

Abstract

The relative contributions that species assemblages, abiotic variables, and their interactions with one another, make to ecosystem properties are recognised but are seldom considered simultaneously, within context, and at the appropriate spatio-temporal
5 scales. Here, we combine fluorescent time-lapse sediment profile imaging (f-SPI) and diffusion gradient thin gels (DGT) to examine, in situ, the link between an important benthic ecosystem process (bioturbation) and ecosystem functioning (trace metal cycling). We show that the mechanistic basis of how the infaunal community mediate Fe and Mn cycles is difficult to reconcile because of the spatio-temporal differences
10 between particle and porewater mixing. This mismatch means that the consideration of these mechanistic processes in isolation is likely to limit our interpretative capacity of how infaunal communities mediate various biogeochemical processes in the natural environment. Moreover, the combination of multiple technologies, process based simulation modelling and generalised additive statistical modelling achieved here, em-
15 phasises the importance of simultaneously considering additional factors that influence benthic chemistry, in particular bioirrigation and tidal flushing of the sediment profile. Our findings highlight a pressing need to determine how the relative importance of multiple abiotic and biotic factors act in concert to alter major biogeochemical pathways across a variety of contexts and habitats.

20 ## 1 Introduction

As it is now accepted that anticipated future declines in marine species abundances, leading to localised species extinctions, will have negative ecological consequences (Worm et al., 2006; Solan et al., 2004a), attention is turning to the prediction of specific ecosystem responses to human activity across a broad range of spatial scales
25 (Halpern et al., 2008; Webb et al., 2009). Highly controlled experiments have been instrumental in formulating a mechanistic understanding of how single (e.g. Duport et al.,

8542

2006) and multiple species (e.g. Emmerson et al., 2001; Marinelli and Williams, 2003; Ieno et al., 2006; Caliman et al., 2007) influence a range of benthic ecosystem functions (Cardinale et al., 2006). In order for these efforts to be relevant to natural systems and the questions that society may pose, however, a portfolio of approaches (Naeem, 2006; Raffaelli, 2006) are required that build upon, and extend from this experimental base (Srivastava and Velland, 2005; Benton et al., 2007). Whilst it is true that inconsistencies between highly controlled experiments and field observations have been overstated (Duffy, 2008), it is known that the contributions species make to ecosystem functioning are context dependent (e.g. Rossi et al., 2008) and are modified by the environment (Bulling et al., 2010; Hicks et al., 2011), although the interdependencies of these influences are often overlooked (Godbold and Solan, 2009).

Numerous examples can be found in the literature on how single environmental variables, such as temperature (Ouelette et al., 2004), food availability (Nogaro, 2008; Maire et al., 2007), light (Rosenberg and Lundberg, 2004), pH (Widdicombe and Needham, 2007), and flow (Solan and Kennedy, 2002; Biles et al., 2002), can act alone, or in concert (Bulling et al., 2010), to modify species contributions to a variety of response variables. Combinations of these factors may lead to non-additive effects (e.g. Folt et al., 1999) which cannot necessarily be predicted from the responses observed under multiple single drivers of change, emphasising the need to examine multiple processes simultaneously (Christensen et al., 2006; Crain et al., 2008). In natural systems, many of these processes will be further influenced in both time and space due to habitat heterogeneity (Dyson et al., 2007; Bulling et al., 2008) and changes in the availability and distribution of resources (Godbold et al., 2011; Jamieson et al., 2011). These temporal and spatial modifications to the environment, in turn, drive the spatial distribution of species (Levinton and Kelaher 2004). Consequently, community composition and diversity may vary depending on prevailing abiotic conditions (Rhoads et al., 1978; Pearson and Rosenberg, 1978; Noren and Lindegarth, 2005) creating a dynamic mosaic of identifiable community patches (Zajac, 2001). These dynamics are reflected in sediment biogeochemical processes (Chapman and Tolhurst, 2007; Teal et al., 2010; Gilbertson

et al., 2012), although the relative importance of the organisms versus the environment in mediating associated sediment function (biogeochemical cycling) can be difficult to distinguish (Godbold and Solan, 2009). It follows, therefore, that in situ observations are necessary to account for the context dependent effects of inter- and intra- specific behaviour, whilst also integrating species-environment interactions (Bulling et al., 2010; Hicks et al., 2011), and will be essential in determining the conditions under which the ecological consequences of change are minimised. Furthermore, the exploration of how local scale processes manifest at regional scales needs to connect with landscape-scale initiatives (Solan et al., 2004a, Webb et al., 2009).

Establishing how multiple factors simultaneously contribute to ecosystem functioning in natural systems is complex, and despite the routine availability of technology (for review, see Solan et al., 2003) that can quantify particular ecosystem functions (e.g. trace metals, Teal et al., 2009; oxygen, Glud et al., 2001; pH and pCO_2, Fan et al., 2011), ecosystem processes (e.g. bioturbation, Solan et al., 2004b; bioirrigation, Forster and Graf, 1995) or infaunal behaviour (Solan and Kennedy, 2002; Maire et al., 2010; Jamieson et al., 2011), inferences gained from each technology remain separate because multiple technologies are seldom used together (Solan et al., 2003). Recent developments in combining multiple in situ methodologies (Teal et al., 2009, 2010; Fan et al., 2011) allow simultaneous acquisition of the necessary high-resolution measurements of ecosystem process and functioning within an environmental context. Here we test whether data gained from the concurrent use of multiple technologies, when examined with analytical techniques that facilitate a mechanistic understanding at the appropriate spatio-temporal scale (simulation models, Schiffers et al., 2011; general additive modelling) provide additional insights into the coupling between ecosystem process (bioturbation) and functioning (trace metal cycling) in a dynamic natural marine system.

2 Materials and methods

2.1 Sediment profile imaging with DGT and fluorescent particle detection

A sediment profile imaging (SPI) camera, incorporating two diffusive gradient in thin film (DGT) gels (each $18.5 \times 2 \times 0.1$ cm) within the faceplate (g-SPI; Teal et al., 2009) was optically modified to allow preferential imaging of fluorescent sediment particles (f-SPI; Solan et al., 2004b, Schiffers et al., 2011). The dimensions of the fg-SPI faceplate were 15×21.5 cm ($= 322.50$ cm^2), but after subtraction of the area occupied by the two DGT gels ($= 74$ cm^2) the field of view reduces to 9×21.5 cm ($= 248.5$ cm^2). The camera (Nikon D100, 2000×3000 pixels $= 6$ mega pixels, effective resolution $= 75 \times 75$ µm per pixel) was set to an exposure of 1/60, $f = 2.0$ and film speed equivalent to ISO 400. The filter, resin gel and diffusive gel needed to make up the DGT sandwich for the detection of trace metals (Fe and Mn) were purchased from DGT Research Ltd (http://www.dgtresearch.com) and prepared following the methodology of Teal et al. (2009). A maximum area 1×17.5 cm gel^{-1} ($n = 3$) is exposed to the sediment during deployment, depending on the depth of fg-SPI prism penetration.

Three replicate time-lapse deployments of the fg-SPI were carried out within a 50 m radius in Loch Creran, West Scotland (centred around $56°31.66'$ N, $5°21.11'$ W), during June–July 2008. The fg-SPI was detached from the research vessel and, to prevent any wind or tidal mediated drag affecting the camera position, the surface buoy was attached to a drop anchor. For each time-lapse sequence, images were taken every 5 min for a period of 96 h ($n = 1152$ images per deployment). Luminophores (~30 g dry weight) were manually spread in front of the SPI faceplate by a SCUBA diver immediately after the camera was deployed (see Supplement Fig. S1a). As high spatial variability in the trace metal profiles was anticipated (Teal et al., 2009), three additional DGT probes (area of gel $= 1.8 \times 15$ cm $= 27$ cm^2) were inserted into the sediment profile to a depth of 11 cm by SCUBA divers within the immediate vicinity (<1 m) of the fg-SPI faceplate (see Supplement Fig. S1b). The DGT probes were stored in sealed Ziplok$^{®}$

plastic bags at $4°C \pm 1°C$ prior to deployment and were attached to the fg-SPI frame using a custom-made PVC holder.

As infaunal activity is known to be influenced by environmental factors, such as flow (Biles et al., 2002) and temperature (Ouelette et al., 2004), a CTD (Saiv A/S STD/CTD, model SD204) and current meter were attached to the fg-SPI to monitor current speed, temperature and the tidal cycle (every 20 s) for the duration of each deployment.

2.2 Site characteristics (SPI and fauna)

An unmodified sediment profile imaging (SPI) camera (for general principles, see Rhoads and Cande, 1971; usage in benthic characterisation reviewed in Germano et al., 2011) was used to obtain in situ images (15×21.5 cm $= 322.50$ cm^2) of the sediment profile to characterise the site based on the image derived mixing depth (MD_I, Teal et al., 2010). The imaging module is based around a Nikon D100 camera (2000×3000 pixels $= 6$ mega pixels, effective resolution $= 75 \times 75$ µm per pixel), set to an exposure of 1/60 and a film speed equivalent to ISO 400. A total of 20 images within a 50 m radius of the sample station were obtained.

The depth of the vertical colour transition (from brown to olive green/black, Lyle, 1983) was delineated using standard threshold analysis of 8-bit (greyscale) tagged image file format (TIFF) images. The upper limit of the region of interest was delineated by the sediment-water interface, whilst the lower limit of the region of interest was determined by using the most appropriate threshold level (user defined) that distinguished the oxidised sediment (high reflectance) from the underlying reduced sediment (low reflectance). The image derived mixing depth (MD_I) is defined as the mean vertical distance of the sediment area that has grey scale intensities above the user-defined threshold value. All image analysis was performed using a custom-made, semi-automated macro (modified from Solan et al., 2004b) within ImageJ (vs 1.40), a Java-based public domain program developed at the USA National Institutes of Health (available at: http://rsb.info.nih.gov/ij/index.html).

To characterize the indicative infaunal community present at the site, macrofauna were identified from the returns of 6 cores ($\varnothing_i$ 10 cm × 10 cm depth, sieved on a 1 mm mesh) taken from within 50 m of the fg-SPI. Fauna were stored in a solution of 4 % formaldehyde buffered with seawater (salinity, 33) and identified to species (75 %) or family (25 %) level. Biomass (g wet weight) was determined to 5 decimal places using an Ohaus Adventurer Pro balance. All fauna were blotted dry with absorbent paper to remove any excess liquid prior to weighing.

2.3 DGT analysis

All DGT sample preparation was undertaken in a laminar flow cabinet (BassAire – Class100). The top membrane and diffusive gel layer were discarded and the resin gel layer was sliced at 2 mm resolution using a teflon coated stainless steel razor blade. Each gel slice was eluted with 2 mol l^{-1} HNO$_3$ (100 μL) for 24 h and then diluted (75 μL sample: 925 μl 2 mol l^{-1} HNO$_3$). 2 mol l^{-1} HNO$_3$ releases 80 % (±4 %) of the metal bound to the Chelex (Zhang et al., 1995). The solutions were analysed for two trace metals (Fe, Mn) using an Agilent Technologies 7500ce Inductively Coupled Plasma-Mass Spectrometer (ICP-MS). The ICP-MS has an octopole reaction system to remove spectral interferences. Fe was analysed in reaction mode (H$_2$) and Mn, in collision mode (He), to remove all the polyatomic spectral interferences. The ICP-MS was calibrated every day prior to the analysis of samples using dilutions (0–200 μg kg^{-1}) of a mixed stock standard (100 mg kg^{-1}). An internal standard of Rh^{103} (50 μg kg^{-1}) was used to check for drift of the machine during the day and a certified reference material (SLRS-4) was used to check the calibrations and recovery of the ICP-MS.

The measured concentrations, C_g (μg kg^{-1}) of the DGT gel solutions were converted to molar concentrations and used to calculate the mass, M (nmol cm^{-2}), accumulated

in the resin layer of each gel strip:

$$M = \left(\frac{C_g(v + V)}{0.8 \times A} \right) \frac{1}{x} \tag{1}$$

where V is the volume of gel (ml), v the extractant volume (ml) and x the atomic mass of the element in question. Knowing the time of gel deployment, t (s), allowed calculation of the time averaged flux F (nmol cm^{-2} s^{-1}) of metal from the porewaters to the resin strip,

$$F = \frac{M}{t \times A} \tag{2}$$

where A is the area of exposed gel (cm^2).

2.4 Image analysis of fluorescent sediment particles

Images were saved in red-green-blue (RGB) colour with JPEG (Joint Photographic Experts Group) compression and analysed using a custom-made, semi-automated macro (Solan et al., 2004b) within ImageJ (version 1.40). The user manually draws in the sediment-water interface on each image and selects an appropriate threshold to select all luminophores. As the primary interest is the vertical distribution of particles relative to the sediment water interface, it is important that depth is measured relative to the sediment-water interface. Therefore, the macro returns a binary matrix (0 = sediment, 1 = luminophores) using the sediment-water interface as the uppermost horizontal row. The total luminophores in each pixel row are then summed to provide the vertical profile of luminophores.

2.5 Statistical analysis

In contrast to previous qualitative methods (Lesven et al., 2008) general additive modelling (GAM, Wood, 2006) was used to determine underlying patterns in the shape

of the replicate Fe and Mn profiles for each deployment. This method is preferential because differences in the shape of replicate profiles and the depth of trace metal flux peaks are of interest, rather than the absolute flux values. GAMs use smoothing curves to model non-linear relationships between the response variable (Fe or Mn flux) and the explanatory variable (depth). Following Wood (2006), thin plate smoothing splines were used to model the non-linearity and the smoothing parameter estimation (degrees of freedom) was optimised using a generalized cross validation procedure. In total, six GAMs were fitted, one for each trace metal (Fe and Mn) across all deployments ($n = 3$). Whilst it can be expected that the heterogeneity between trace metal profiles is large enough for single smoothers to be fitted to each individual profile (Teal et al., 2009), our objective is to establish whether an underlying trend may link directly to infaunal activity levels. Hence, only one smoother was fitted with depth for each GAM, rather than modelling the full heterogeneity in flux patterns using multiple smoothers. Both Fe and Mn flux were cube-root transformed to reduce the influence of peaks in absolute values on the underlying smoother trends. Profile identity (hereafter, profile ID) was fitted as a nominal variable to account for differences in absolute flux values between replicates. All models were validated by visual comparison of residual plots and final models were used to predict Fe and Mn flux profiles with depth for each deployment. These predicted profiles were then compared to observed vertical distributions of bioturbation activity (luminophore profiles).

2.6 Bioturbation model

Luminophore profiles obtained from hourly images ($n = 94$ per deployment) in the fg-SPI sequences were analysed using a process based simulation model (Schiffers et al., 2011). The output parameters of the simulation model, *activity, tracerdif*, and *distance*, describe the mechanistics of the observed particle displacement (*activity* = the probability that a luminophore pixel will be displaced between two timesteps; *distance* = the mean distance of the particle displacement between each time step; and *tracerdif* is used as a weighting parameter to account for any differences in specific density

8549

between the luminophore tracer and the sediment that may change the probability of passive tracer displacement, Schiffers et al., 2011). Use of the simulation model is preferential to other ways of interpreting tracer profiles, such as the calculation of bioturbation coefficients (see review by Meysman et al., 2008), because the short duration of the experiment (5 days) means that the underlying assumptions behind the calculation of bioturbation coefficients are violated. Following Schiffers et al. (2011), the optimal combination of parameter values, i.e. where the sum of squares reached a minimum, were identified using the "optim" function implemented in the "R" statistical and programming environment (R Development Core Team 2008). The final fitting procedure was repeated 5 times to obtain mean parameter estimates and corresponding error estimation.

3 Results

3.1 Loch Creran site characteristics and faunal assemblage

Sea state was comparable (calm) for all three deployments. Temperatures and salinities showed a mean (±SD) of $12.12 \pm 0.13\,^\circ$C and 33.57 ± 0.06 respectively during deployment 1, $12.35 \pm 0.07\,^\circ$C and 33.39 ± 0.13 during deployment 2 and $12.45 \pm 0.08\,^\circ$C and 33.53 ± 0.12 during deployment 3. All deployments were carried out at 13 m water depth, but the tidal influence meant that the depth ranged from 11.7–13.9 m during deployment 1, from 11.2–14.6 m during deployment 2 and from 11.3–14.5 m during deployment 3.

The SPI survey of the site ($n = 20$) immediately prior to the fg-SPI deployments, revealed a mean (±SD) sediment mixing depth (MD_l) of 3.7 ± 0.9 cm ($n = 20$, range = 2.6–5.9 cm). Infaunal burrows were consistently present, showing evidence of high bioturbation activity and considerable spatial heterogeneity of the sediment environment. The faunal returns indicated a species rich community characterised by *Abra nitida*, *Amphiura chiajei* and *Terrebellidae* spp. These species were consistently found across

8550

replicate samples (Table 1). *Turritella communis* and *A. chiajei* were biomass dominants followed closely by *A. nitida*, *Terrebellidae* sp. 1 and the Capitellids *Heteromastus filiformis* and *Notomastus latericus* (Table 1). Although *T. communis* was not present across all samples, evidence from SCUBA diver photography (Fig. S2) indicated that this species was present in high abundance.

3.2 Particle bioturbation

The time lapse f-SPI sequences showed considerable variability between deployments (Figs. 1 and 2), reflecting temporal differences in species composition and species behaviour during the sequence. In deployment 1 (Fig. 2a) the initial surficial layer of luminophores remained largely undisturbed for an extended period of time (∼60 h), although a small downward movement most likely related to the upward extension of *Amphiura* spp. (based on Table 1, most likely *Amphiura chiajei*) feeding "arms" was observed. An immediate change in luminophore distribution occurs at ∼3800 min (60 h), following the appearance of a decapod Crustacean (most likely *Carcinus maenas*) that mixes sediment to a depth >2 cm. Consistent with the findings of Solan et al. (2004b), this event masks the effect of *Amphiura* spp., which were active throughout the time-lapse sequence.

In deployment 2, particle mixing to 1.5 to 2 cm occurs more rapidly than during deployment 1 and an initial subduction of luminophores is evident at ∼600 min (10 h) following feeding activity by one individual of *Turritella communis* (Figs. 2b and 1). A further downward injection of luminophores is evident at ∼1500 min (25 h, Fig. 2b), which is related to the presence of a decapod crustacean (most likely *Carcinus maenas*) and other epifauna (e.g. *Asterias rubens*, *Crangon* sp. and a *Gobiidae* species). Burrowing at depths below the level of luminophore incorporation (>5 cm) also occurred, although it was not possible to confirm which species were active at these depths.

The greatest redistribution of luminophores occurred during deployment 3 (Fig. 2c). The most striking bioturbation events occurred at ∼560 min (9.3 h), ∼1000 min (16.7 h) and ∼3000 min (50 h, Fig. 2c). Closer examination of the image sequence reveals that

8551

these events were associated with decapod crustacean activity, including the construction of a large burrow (∼2 cm deep) at an elapsed deployment time of 1000 min. Nevertheless, there was considerable redistribution of luminophores occurring within the sediment profile (Fig. 2c), largely associated with the burrowing and feeding behaviour of *Amphiura* spp. (based on table 1 most likely *Amphiura chiajei*) and Nereidae spp.

A strong correlation was found between the bioturbation parameters *activity* and *distance* (Fig. S3a–c), indicating that there was not a unique global minimum in parameter space. However, as this preliminary optimisation indicated the optimal value for the parameter *activity* (= 0.99, deployment 1; 0.99, deployment 2; 0.98, deployment 3), *activity* was fixed at these respective values (following Schiffers et al., 2011), to aid the appropriate optimization of the values for *tracerdif* and *distance*. Model simulations showed acceptable levels of fit (Fig. S4) and parameter estimations showing very low variability (Table 2). The mean distance of particle displacement to be $75 \pm 1 \, \mu m \, hr^{-1}$ (deployment 1), $181 \pm 9 \, \mu m \, hr^{-1}$ (deployment 2) and $390 \pm 43 \, \mu m \, hr^{-1}$ (deployment 3). It is important to emphasise that these are not net downward movements but the average of both upward and downward movements across the time period of observation. Values for *tracerdif* were similar during deployment 2 (0.901 ± 0.037) and deployment 3 (0.958 ± 0.062), but significantly larger than both these deployments (t-test, $p < 0.001$) during deployment 1 (0.790 ± 0.007), indicating some variation in tracer behaviour relative to sediment particles. *Activity*, the probability of particle displacement, returned a high value (>0.9) for all three deployments, indicating the presence of continuous mixing.

3.3 Distribution of Fe and Mn

The absolute values and the depth of the profile peaks varied greatly for both Fe and Mn between deployments as well as between replicate profiles within the same deployment (Fig. 3a–f). Nevertheless, with the exception of the considerable variability in Fe profile shape during deployment 1 (Fig. 3a), it was possible to establish underlying trends in the distribution of peaks between profiles within each deployment. Following

8552

the sequential utilisation of electron acceptors, Mn peaks are observed at shallower depths (~1–4 cm) relative to the Fe peaks (~4–8 cm) and both metals decrease in concentration below their respective peaks. The variability between profiles is most pronounced around the main subsurface peaks, indicating considerable heterogeneity (at the µm scale) within the sediment leading to variable depths (2–10 cm) of peak trace metal release into pore waters.

The relationship between Fe and Mn (Fig. 4) shows no pattern and it was not possible to clearly distinguish the Mn reduction zone from the Fe reduction zone. Thus, a segmented regression analysis to determine the depth of the Fe redox boundary (as in Teal et al., 2009) was not suitable. The inability to define the Fe-Mn relationship most likely relates to the heterogeneity observed between individual profiles within a single deployment (Fig. 3) that, in turn, reflect variation in the type, duration and frequency of bioturbation events.

3.4 Linking trace metal profiles and bioturbation

All six GAMs fitted to Fe and Mn profiles of each deployment showed significant smoothers ($p < 0.01$ in all cases, $df = 3$ in all cases except for Fe deployment 2, where $df = 4$) as well as a significant difference between replicates ($p < 0.01$ in all cases), indicating that absolute flux values differed significantly between replicate location. Despite the difference in absolute values, it was possible to detect an underlying trend (smoother) in the shape of the profiles for each deployment and each metal. Based on the output, flux values (±SD) of both Fe and Mn could be calculated to compare with luminophore distributions.

Predicted Fe and Mn flux profiles with sediment depth based on GAM show a gradual increase in fluxes at the sediment surface with flattened peaks at mid-depths (between 2–8 cm), gradually decreasing with depth (Fig. 5). Although the curves do not reveal any distinct depth-specific peaks in either Fe or Mn, it is evident that Fe reaches maximal concentrations between 4–8 cm (Fig. 5a, c, e), and that Mn reaches maximal concentrations between 1–4 cm (Fig. 5b, d, f). This pattern is consistent with a priori

predictions based on biogeochemical zonation theory, i.e. as an electron acceptor, Mn > Fe (Aller, 1982). The flattened shape of the curves and lack of a distinct peak for Fe and Mn reflect the variability in peaks between profiles, as well as the heterogeneity within profiles, which are averaged in the GAM analysis.

It is important to consider the shape of the Fe and Mn profiles in relation to the vertical distribution of luminophores. Over the time-period of observation, the luminophore profile remains limited to the upper 2 cm of the sediment profile, consistent with the depth region of Mn release (Fig. 5). The "noise" and slightly deeper penetration of luminophores in deployment 3 can be related to more intense bioturbation activity (Fig. 5c), which may have caused a downwards shift in the location of the peak concentrations of both Mn and Fe, i.e. extended regions of Fe and Mn release. This view is supported by deployment 1, where a more defined and sharper peak in Fe (Fig. 5a) reflects a less noisy luminophore profile and is associated with less active bioturbation and smaller mean particle displacements.

4 Discussion

Although the sediment mixing depth provides a good proxy of broad scale sediment function, integrating both biotic and abiotic processes (Teal et al., 2010), it is necessary to understand the intimate association between biotic and abiotic processes at the small scale before broader scale patterns and processes can be appreciated. For example, the theoretical vertical zonation of biogeochemical reactions within the sediment are known to be perturbed by infaunal activities, creating a mosaic of oscillating redox microniches within the sediment (Aller, 1984). Recent studies have qualitatively linked the degree of the disruption of redox zones to infaunal activity levels (Bertics and Ziebis, 2009; Teal et al., 2009) and it is clear that sediment microniches significantly contribute to the observed variability between trace metal profiles (Stockdale et al., 2009). In this study, it appears that layered biogeochemical depth zones have been disrupted, i.e. oxidation of both Fe and Mn is occurring at variable depths and across

a small spatial scale. These patterns can be directly related to the spatio-temporal variability in bioturbation activity, both vertically and horizontally within the sediment, creating a four-dimensional dynamic mosaic of environmental conditions. The effects of bioturbation on nutrient cycling are well documented (e.g. Ieno et al., 2006; Dunn et al., 2009), and are known to be influenced by many abiotic factors, but the interdependencies of faunal behaviour and nutrient cycles have only recently been qualitatively linked in laboratory (Gilbertson et al., 2012) and in situ experiments (Volkenborn et al., 2007; Glud et al., 2009; Godbold and Solan, 2009; Teal et al., 2009; Teal et al., 2010).

The most striking feature of this study was the pronounced variation in both infaunal bioturbatory activity and trace metal cycling, even at relatively short distances of a few cm. The difficulty of determining the shape of sediment particle and porewater associated trace metal profiles highlights an intrinsic difficulty in investigating and quantifying organism-process-function relations in a natural environment. Species-environment interactions are context-dependent (Rossi et al., 2008) and thus relations within transient natural communities are extremely variable in both time and space. Even on small spatial scales (within a 50 m diameter study site) and with temporal averaging (over a 5 day period), it is clear that levels and types of bioturbation observed are largely dependent on the temporal dynamics of assemblage structure, presumably including changes in behaviour resulting from species interactions (Maire et al., 2010). Whilst this is not surprising, it is important to highlight that in most in situ studies of bioturbation the variability in faunal structure and environmental conditions are routinely ignored and average effects are reported that mask the effects of certain circumstances. Here, the use of imaging technology coupled with multiple environmental sensors meant that discrete bioturbation events (sensu Solan et al., 2004b) can be directly related to species-specific behaviour (i.e. locomotion by *C. maenas*, feeding by *T. communis*, burrowing by *A. filiformis*) and/or environmental conditions (e.g. ebb and flow of the tide, Solan and Kennedy, 2002). These observations underpin the parameter values of the bioturbation simulation model, as the highest activity and distances that particles are displaced will be strongly affected by such discrete events, yet previous work has underestimated

their functional importance and structural role. It is clear, therefore, that extended and detailed observations are required to fully evaluate and integrate the modifying effects of tidal (Solan and Kennedy, 2002; Biles et al., 2002) and day-night cycles (Rosenberg and Lundberg, 2004), as well as the effects of intra- and inter-specific interactions (Ieno et al., 2006; Caliman et al., 2007) on net benthic process (bioturbation). Indeed, understanding how benthic process-function relations alter under specific circumstances is likely to provide insight into the likely ecological consequences of anticipated environmental change (Bulling et al., 2010; Hicks et al 2011).

Despite the high degree of variability detected between replicate trace metal profiles, we were able to fit smoothers that indicate that a consistent underlying pattern of Mn reduction and Fe reduction zones does exist across replicates, regardless of fundamental differences in the type and amount of bioturbation. The difficulty of linking particle movement patterns and trace metal profiles may, however, be explained partly by the disconnect between the spatio-temporal scales over which particle movement and porewater bioirrigation operate. Whilst luminophore profiles take an extended time period (hours to days, e.g. Teal, 2009) to establish a homogenous distribution within the most actively mixed sediment layer, trace metal profiles form more rapidly because they integrate changes in the sediment pore water concentrations that oscillate on much shorter time-scales (e.g. Forster and Graf, 1995), immediately reacting to influxes of oxygenated water (Wethey et al., 2008; Shull et al., 2009). Furthermore, porewater chemistry can be affected by processes not considered here, in particular tidal currents at the large scale (Kuwae et al., 2003) and bioirrigation at smaller scales (Waldbusser and Marinelli, 2006; Na et al., 2008; Shull et al., 2009). Nevertheless, the fact that we have detected a generic series of mechanisms that link ecosystem process to functioning in the presence of substantial variation and differences in the scales of *modus operandi*, suggests that with appropriate multidisciplinary collaboration the same can be achieved at larger scales despite perceived practical constraints (Raffaelli et al., 2005; Benton et al., 2007). Thus, the immediate challenge in understanding species-process-function-environment relations is to reconcile effects observed at small scale

and under specific circumstances with the consistent and general effects that operate at larger temporal and spatial scales, associated with, for example, environmental change.

Supplementary material related to this article is available online at: http://www.biogeosciences-discuss.net/9/8541/2012/ bgd-9-8541-2012-supplement.zip.

References

Aller, R. C.: The effects of macrobenthos on chemical properties of marine sediments and overlying water, in: Animal-Sediment Relations, the Biogenic Alteration of Sediments, edited by: Call, P. L. and Tevesz, M. J. S., Plenum Press, New York, 53–102, 1982.

Aller, R. C.: The importance of relict burrow structures and burrow irrigation in controlling sedimentary solute distributions, Geochim. Cosmochim. Ac., 48, 1929–1934, 1984.

Benton, T. G., Solan, M., Travis, J. M. J., and Sait, S. M.: Microcosm experiments can inform global ecological problems, Trends Ecol. Evol., 22, 516–521, 2007.

Bertics, V. J. and Ziebis, W.: Biodiversity of benthic microbial communities in bioturbated coastal sediments is controlled by geochemical microniches, ISME J., 3, 1269–1285, 2009.

Biles, C. L., Paterson, D. M., Ford, R. B., Solan, M., and Raffaelli, D. G.: Bioturbation, ecosystem functioning and community structure, Hydrol. Earth Syst. Sci., 6, 999–1005, doi:10.5194/hess-6-999-2002, 2002.

Bulling, M. T., Solan, M., Dyson, K. E., Hernandez-Milian, G., Luque, P., Pierce, G. J., Raffaelli, D., Paterson, D. M., and White, P. C. L.: Species effects on ecosystem processes are modified by faunal responses to habitat composition, Oecologia, 158, 511–520, 2008.

Bulling, M. T., Hicks, N., Murray, L., Paterson, D. M., Raffaelli, D., White, P. C. L., and Solan, M.: Marine biodiversity-ecosystem functions under uncertain environmental futures, Philos. T. Roy. Soc. B, 365, 2107–2116, 2010.

Caliman, A., Leal, J. J. F., Esteves, F. A., Carneiro, L. S., Bozelli, R. L., and Farjalla, V. F.: Functional bioturbator diversity enhances benthic-pelagic processes and properties in experimental microcosms, J. N. Am. Benthol. Soc., 26, 450–459, 2007.

Cardinale, B. J., Srivastava, D. S., Duffy, J. E., Wright, J. P., Downing, A. L., Sankaran, M., and Jouseau, C.: Effects of biodiversity on the functioning of trophic groups and ecosystems, Nature, 443, 989–992, 2006.

Chapman, M. G. and Tolhurst T. J.: Relationships between benthic macrofauna and biogeochemical properties of sediments at different spatial scales and among different habitats in mangrove forests, J. Exp. Mar. Biol. Ecol., 343, 96–109, 2007.

Christensen, M. R., Graham, M. D., Vinebrooke, R. D., Findlay, D. L., Paterson, M. J., and Turner, M. A.: Multiple anthropogenic stressors cause ecological surprises in boreal lakes, Global Change Biol., 12, 2316–2322, 2006.

Crain, C. M., Kroeker, K., Halpern, B. S.: Interactive and cumulative effects of multiple human stressors in marine systems, Ecol. Lett., 11, 1304–1315, 2008.

Duffy, J. E.: Why biodiversity is important to the functioning of real-world ecosystems, Front. Ecol. Environ., 7, 437–444, 2008.

Dunn, R. J. K., Welsh, D. T., Jordan, M. A., Teadale, P. R., and Lemckert, C. J.: Influence of natural amphipod (*Vitoriopisa asutraliensis*) (Chilton, 1923) population densities on benthic metabolism, nutrient fluxes, denitrification and DNRA in sub-tropical estuarine sediment, Hydrobiologia, 628, 95–109, 2009.

Duport, E., Stora, G., Tremblay, P., and Gilbert, F.: Effects of population density on the sediment mixing induced by the gallery-diffusor *Hediste (Nereis) diversicolor*, O. F. Müller, 1776, J. Exp. Mar. Biol. Ecol., 336, 33–41, 2006.

Dyson, K. E., Bulling, M. T., Solan, M., Hernandez-Milian, G., Raffaelli, D. G., White, P. C. L., and Paterson, D. M.: Influence of macrofaunal assemblages and environmental heterogeneity on microphytobenthic production in experimental systems, P. Roy. Soc. Lond. B Bio., 274, 2547–2554, 2007.

Emmerson, M. C., Solan, M., Emes, C., Paterson, D. M., and Raffaelli, D.: Consistent patterns and the idiosyncratic effects of biodiversity in marine ecosystems, Nature, 411, 73–77, 2001.

Fan, Y., Zhu, Q., Aller, R. C., and Rhoads, D. C.: An in situ multispectral imaging system for planar optodes in sediments: examples of high-resolutions seasonal patterns of pH, Aquat. Geochem., 17, 457–471, 2011.

Folt, C. L., Chen, C. Y., Moore, M. V., and Burnaford, J.: Synergism and antagonism among multiple stressors, Limnol. Oceanogr., 44, 864–877, 1999.

Forster, S. and Graf, G.: Impact of irrigation on oxygen flux into the sediment: intermittent pumping by *Callianassa subterranea* and "piston-pumping" by *Lanice conchilega*, Mar. Biol., 123, 335–346, 1995.

Germano, J. D., Rhoads, D. C., Valente, R. M., Carey, D. A., and Solan, M.: The use of Sediment Profile Imaging (SPI) for environmental impact assessments and monitoring studies: lessons learned from the past four decades, Oceanogr. Mar. Biol., 49, 235–298, 2011.

Gilbertson, W. W., Solan, M., Prosser, J. I.: Differential effects of microbe-invertebrate interactions on benthic nitrogen cycling, FEMS Microbiol. Ecol., doi:10.1111/j.1574–6941.2012.01400.x, accepted, 2012.

Glud, R. N., Tengberg, A., Kuhl, M., Kall, P. O. J., Klimant, I., and Host, G.: An in situ instrument for planar O_2 optode measurements at benthic interfaces, Limnol. Oceanogr., 46, 2073–2080, 2001.

Glud, R. N., Thamdrup, B., Stahl, H., Wenzhoefer, F., Glud, A., Nomaki, H., Oguri, K., Revsbech, N. P., and Kitazato, H.: Nitrogen cycling in a deep ocean margin sediment (Sagami Bay, Japan), Limnol. Oceanogr., 54, 723–734, 2009.

Godbold, J. A. and Solan, M.: Relative importance of biodiversity and the abiotic environment in mediating ecosystem process, Mar. Ecol.-Prog. Ser., 396, 273–282, 2009.

Godbold, J. A., Bulling, M. B., and Solan, M.: Habitat structure mediates biodiversity effects on ecosystem properties, P. Roy. Soc. Lond. B Bio., 278, 2510–2518, 2011.

Halpern, B. S., Walbridge, S., Selkoe, K. A., Kappel, C. V., Micheli, F., D'Agrosa, C., Bruno, J. F., Casey, K. S., Ebert, C., Fox, H. E., Fujita, R., Heinemann, D., Lenihan, H. S., Madin, E. M. P.,

Perry, M. T., Selig, E. R., Spalding, M., Steneck, R., and Watson, R.: A global map of human impact on marine ecosystems, Science, 319, 948–952, 2008.

Hicks N., Bulling M. T., Solan M., Raffaelli D., White P. C. L., and Paterson, D. M.: Impact of biodiversity-climate futures on primary production and metabolism in a model benthic estuarine system, BMC Ecology, 11, , 8 pp., doi:10.1186/1472-6785-11-7, 2011. article number: Total pages = 8

Ieno, E. N., Solan, M., Batty, P., and Pierce, G. J.: How biodiversity affects ecosystem functioning: roles of infaunal species richness, identity and density in the marine benthos, Mar. Ecol.-Prog. Ser., 311, 263–271, 2006.

Jamieson, A. J., Gebruk, A., Fujii, T., and Solan, M.: Functional effects of the hadal sea cucumber *Elpidia atakama* (*Echinodermata: Holothuroidea, Elasipodia*) reflect small-scale patterns of resource availability, Mar. Biol., 158, 2695–2703, 2011.

Kuwae, T., Kibe, E., and Nakamura, Y.: Effect of emersion and immersion on the porewater nutrient dynamics of an intertidal sandflat in Tokyo Bay, Estuar. Coast. Shelf S., 57, 929–940, 2003.

Lesven, L., Gao, Y., Billon, G., Leermakers, M., Ouddane, B., Fischer, J. C., and Baeyens, W.: Early diagenetic processes aspects controlling the mobility of dissolved trace metals in three riverine sediment columns, Sci. Total Environ., 407, 447–459, 2008.

Levinton, J. and Kelaher, B.: Opposing forces of deposit-feeding marine communities, J. Exp. Mar. Biol. Ecol., 300, 65–82, 2004.

Lyle, M.: The brown-green colour transition in marine sediments: a marker of the Fe(III)-Fe(II) redox boundary, Limnol. Oceanogr., 28, 1026–1033, 1983.

Maire, O., Duchêne, J.-C., Bigot, L., and Greìmare, A.: Linking feeding activity and sediment reworking in the deposit-feeding bivalve Abra ovata with image analysis, laser telemetry, and luminophore tracers, Mar. Ecol.-Prog. Ser., 351, 139–150, 2007.

Maire, O., Merchant, J. N., Bulling, M., Teal, L. R., Grémare, A., Duchêne, J. C., and Solan, M.: Indirect effects of non-lethal predation on bivalve activity and sediment reworking, J. Exp. Mar. Biol. Ecol., 395, 30–36, 2010.

Marinelli, R. L. and Williams, T. J.: Evidence for density-dependant effects of infauna on sediment biogeochemistry and benthic-pelagic coupling in nearshore systems, Estuar. Coast. Shelf S., 57, 179–192, 2003.

Meysman, F. J. R. Malyuga, V. S., Boudreau, B. P., and Middelburg, J. J.: A generalized stochastic approach to particle dispersal in soils and sediments, Geochim. Cosmochim. Ac., 72, 3460–3478, 2008.

Na, T., Gribsholt, B., Galaktionov, O. S., Lee, T., and Meysman, F. J. R.: Influence of advective bio-irrigation on carbon and nitrogen cycling in sandy sediments, J. Mar. Res., 66, 691–722, 2008.

Naeem, S.: Expanding scales in biodiversity-based research: challenges and solutions for marine systems, Mar. Ecol.-Prog. Ser., 311, 273–283, 2006.

Nogaro. G., Charles, F., Brage de Mendonça Jr, J., Mermillod-Blondin, F., Stora, G., and François-Carcaillet, F.: Food supply impacts sediment reworking by *Nereis diversicolor*, Hydrobiologia, 598, 403–408, 2008.

Noren, K. and Lindegarth, M.: Spatial, temporal and interactive variability of infauna in Swedish coastal sediments, J. Exp. Mar. Biol. Ecol., 317, 53–68, 2005.

Ouelette, D., Desrosiers, G., Gagne, J.-P., Gilbert, F., Poggiale, J. C., Blier, P. U., and Stora, G.: Effects of temperature on in vitro sediment reworking processes by a gallery biodiffusor, the polychaete *Neanthes virens*, Mar. Ecol.-Prog. Ser., 266, 185–193, 2004.

Pearson, T. H. and Rosenberg, R.: Macrobenthic succession in relation to organic enrichment and pollution of the marine envorinment, Oceanogr. Mar. Biol., 16, 229–311, 1978.

R Development Core Team: R: A Language and Environment for Statistical Computing, R Foundation for Statistical Computing, Vienna, Austria, available at: http://www.R-project.org, 2008.

Raffaelli, D. G.: Biodiversity and ecosystem functioning: issues of scale and trophic complexity, Mar. Ecol.-Prog. Ser., 311, 285–294, 2006.

Raffaelli, D., Solan, M., and Webb, T. J.: Do marine ecologists do it differently?, Mar. Ecol.-Prog. Ser., 304, 283–289, 2005.

Rhoads, D. C. and Cande, S.: Sediment profile camera for in situ study of organism-sediment relations, Limnol. Oceanogr., 16, 110–114, 1971.

Rhoads, D. C., McCall, P. L., and Yingst, J. Y.: Disturbance and production on the estuarine sea floor, Am. Sci., 66, 577–586, 1978.

Rosenberg, R. and Lundberg L.: Photoperiodic activity pattern in the brittle star *Amphiura filiformis*, Mar. Biol., 145, 651–656, 2004.

Rossi, F., Gribsholt, B., Middelburg, J. J., and Heip, C.: Context-dependent effects of suspension feeding on intertidal ecosystem functioning, Mar. Ecol.-Prog. Ser., 354, 47–57, 2008.

Schiffers, K., Teal, L. R., Travis, J., and Solan, M.: Fitting a simulation model to highly resolved spatio-temporal bioturbation data, PLoS ONE, 6, e28028, doi:10.1371/journal.pone.0028028, 2011.

Shull, D. H., Benoit, J. M., Wojcik, C., and Senning J. R.: Infaunal burrow ventilation and porewater transport in muddy sediments, Estuar. Coast. Shelf S., 83, 277–286, 2009.

Solan, M. and Kennedy, R.: Observation and quantification of in-situ animal-sediment relations using time-lapse sediment profile imagery (t-SPI), Mar. Ecol.-Prog. Ser., 228, 179–191, 2002.

Solan, M., Germano, J. D., Rhoads, D. C., Smith, C., Michaud, E., Parry, D., Wenzhofer, F., Kennedy, B., Henriques, C., Battle, E., Carey, D., Iocco, L., Valente, R., Watson, J., and Rosenberg, R.: Towards a greater understanding of pattern, scale and process in marine benthic systems: a picture is worth a thousand worms, J. Exp. Mar. Biol. Ecol., 285, 313–338, 2003.

Solan, M., Cardinale, B. J., Downing, A. L., Engelhardt, K. A. M., Ruesink, J. L., and Srivastaca, D. S.: Extinction and ecosystem function in the marine benthos, Science, 206, 1177–1180, 2004a.

Solan, M., Wigham, B. D., Hudson, I. R., Kennedy, R., Coulon, C. H., Norling, K., Nilsson, H. C., and Rosenberg, R.: In-situ quantification of bioturbation using time-lapse fluorescent sediment profile imaging (f-SPI), luminophore tracers and model simulation, Mar. Ecol.-Prog. Ser., 271, 1–12, 2004b.

Srivastava, D. S. and Velland, M.: Biodiversity-ecosystem function research: is it relevant to conservation?, Annu. Rev. Ecol. Evol. S., 36, 267–294, 2005.

Stockdale, A., Davison, W., and Zhang, H.: Micro-scale biogeochemical heterogeneity in sediments: a review of available technology and observed evidence, Earth Sci. Rev., 92, 81–97, 2009.

Teal, L. R.: The influence of infaunal bioturbation on ecosystem processes in the sediment mixed layer, PhD Thesis, University of Aberdeen, 2009.

Teal, L. R., Parker, E.R, Fones, G., and Solan, M.: Simultaneous determination of vertical transitions of colour, porewater metals and visualization of infaunal activity in marine sediments, Limnol. Oceanogr., 54, 1801–1810, 2009.

Teal, L. R., Parker, E. R., and Solan, M.: The sediment mixed layer as a proxy for measuring benthic ecosystem process and function, Mar. Ecol.-Prog. Ser., 414, 27–40, 2010.

Volkenborn, N., Hedtkamp, S. I. C., van Beusekorn, J. E. E.m, and Reise, K.: Effects of bioturbation and bioirrigation by lugworms (*Arenicola marina*) on physical and chemical sediment properties and implications for intertidal habitat succession, Estuar. Coast. Shelf S., 74, 331–343, 2007.

Waldbusser, G. G. and Marinelli, R. L.: Macrofaunal medication of porewater advection: role of species function, species interaction, and kinetics, Mar. Ecol.-Prog. Ser., 311, 217–231, 2006.

Webb, T. J., Aleffi, I. F., Amouroux, J. M., Bachelet, G., Degraer, S., Dounas, C., Fleischer, Dirk, Gremare, A., Herrmann, M., Hummel, H., Karakassis, I., Kedra, M., Kendall, M. A., Kotwicki, L., Labrune, C., Nevrova, E. L., Occhipinti-Ambrogi, A., Petrov, A., Revkov, N. K., Sarda, R., Simboura, N., Speybroeck, J., Van Hoey, G., Vincx, M., Whomersley, P., Willems, W., and Wlodarska-Kowalczuk, M.: Macroecology of the European soft sediment benthos: insights from the MacroBen database, Mar. Ecol.-Prog. Ser., 382, 287–296, 2009.

Wethey, D. S., Woodin, S. A., Volkenborn, N., and Reise, K.: Porewater advection by hydraulic activities of lugworms, *Arenicola marina*: a field, laboratory and modelling study, J. Mar. Res., 66, 255–273, 2008.

Widdicombe, S. and Needham, H. R.: Impact of CO_2-induced seawater acidification on the burrowing activity of *Nereis virens* and sediment nutrient flux, Mar. Ecol.-Prog. Ser., 341, 111–122, 2007.

Wood, S. N.: Generalised Additive Modelling: An Introduction in R, Chapman and Hall, Boca Raton, Florida, United States, 2006.

Worm, B., Barbier, E. B., Beaumont, N., Duffy, J. E., Folke, C., Halpern, B. S., Jackson, J. B. C., Lotze, H. K., Micheli, F., Palumbi, S. R., Sala, E., Selkoe, K. A., Stachowitz, J. J., and Watson, R.: Impacts of biodiversity loss on ocean ecosystem services, Science, 314, 787–790, 2006.

Zajac, R. N.: Organism-sediment relations at multiple spatial scales: implications for community structure and successional dynamics, in: Organism-Sediment Interactions, edited by: Aller, J. Y., Woodin, S. A., and Aller, R. C., University of South Carolina Press, Columbia, SC, 119–139, 2001.

Zhang, H., Davison, W., Miller, S., and Tych, W.: In situ high resolution measurements of fluxes of Ni, Cu, Fe, and Mn and concentrations of Zn and Cd in porewaters by DGT, Geochim. Cosmochim. Ac., 59, 4181–4192, 1995.

Table 1. Summary of mean species abundance (A ± SD) and biomass (B, g ± SD) per m^2 at the Loch Creran sampling site. N shows the total number of samples where each species was present (N_{total} = 6).

Species	A	±SD	B	±SD	N
Abra nitida	132.63	6.03	0.5181	1.2956	3
Amphipoda	5.31	–	0.0078	–	1
Amphiura chiajei	42.44	36.75	6.9845	6.8296	4
Capitellidae sp.	5.31	–	0.0179	–	1
Corbula gibba	5.31	–	0.0477	–	1
Cylichna cylindracea	10.61	0.00	0.0452	0.0099	2
Euclymene robusta	10.61	–	0.1846	–	1
Eumida sanguinea	5.31	–	0.0025	–	1
Heteromastus filiformis	15.92	22.51	0.2553	0.5204	2
Magelone mirabilis	5.31	–	0.0001	–	1
Maldane sarsi	5.31	–	0.0204	–	1
Notomastus latericus	10.61	0.00	0.3021	0.6808	2
Nucula nitidosa	10.61	0.00	0.0838	0.1621	2
Odostomia sp.	10.61	–	0.0075	–	1
Phyllodocidae	5.31	–	–	–	1
Polychaete fragments	–	–	0.1446	–	1
Sabellidae	10.61	–	0.1407	–	1
Scalibregma inflatum	26.52	36.75	0.0879	0.2456	3
Terrebellidae sp. 1	37.14	36.75	0.5797	1.3027	2
Terrebellidae sp. 2	10.61	–	0.0075	–	1
Thracia pubescens	5.31	–	0.3728	–	1
Turritella communis	15.92	0.71	13.2635	53.4996	2

Table 2. Summary of the replicate ($n = 5$) runs of the BFGS fitting procedure for each fg-SPI deployment for the estimated parameters *distance* and *tracerdif*. As a preliminary optimisation revealed a strong correlation between *activity* and *distance*, *activity* was fixed as indicated for each deployment.

Depl	activity	Run	distance	tracerdif
		1	75.40	0.7898
		2	75.40	0.7846
1	0.9903	3	75.28	0.7741
		4	75.16	0.7898
		5	75.48	0.7909
		1	180.71	0.9010
		2	184.26	0.9894
2	0.9118	3	179.64	0.9292
		4	193.50	0.9778
		5	202.81	0.9669
		1	409.72	0.9515
		2	409.69	0.9952
3	0.9823	3	408.74	0.9969
		4	313.50	0.8519
		5	409.65	0.9952
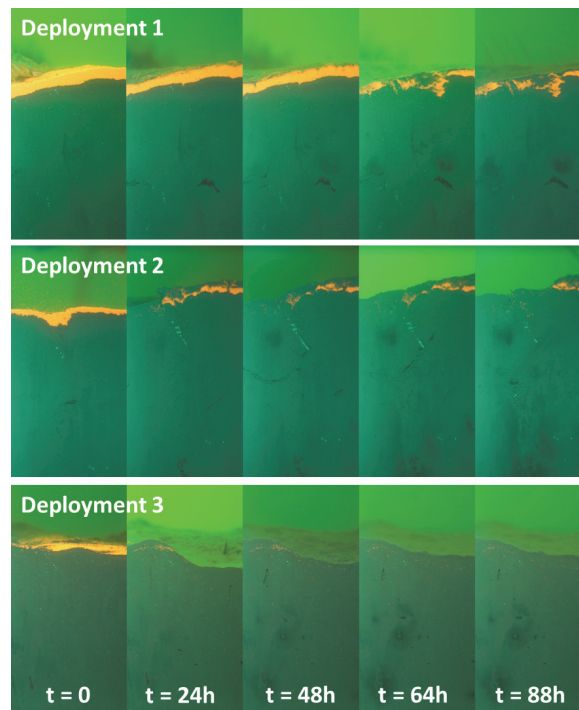
Fig. 1. Selected images from the SPI time-lapse sequence detailing the impact of bioturbation on luminophore particle displacement during the three separate deployments showing a frame for each 24 h period starting from frame 1 ($t = 0$ min). Luminophore particles appear as orange against the sediment in dark green. Scale: frame width = 7 cm.
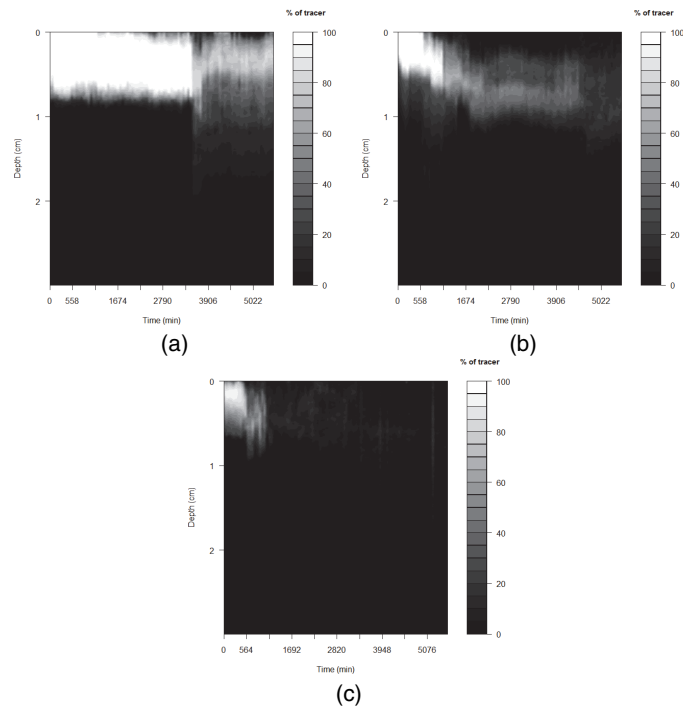
Fig. 2. The redistribution of luminophore particle tracers over time for **(a)** deployment 1, **(b)** deployment 2 and **(c)** deployment 3 of the fg-SPI. Luminophore counts are expressed relative to the total recovered from each image (%) and represented by grey scale shading.

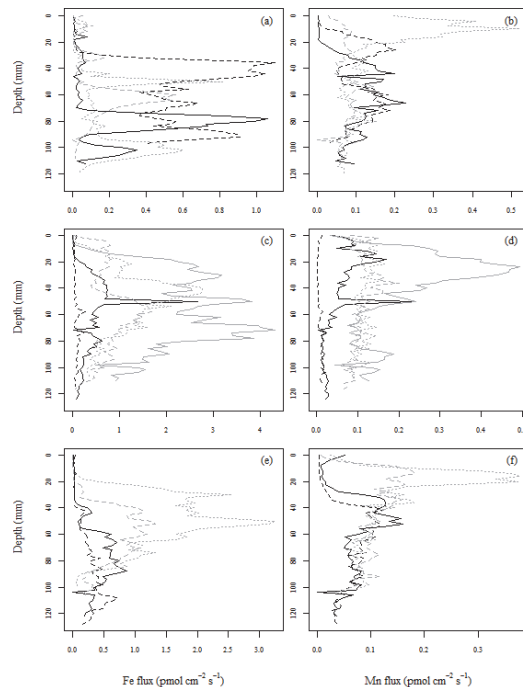**Fig. 3.** Sediment profiles of trace metal flux for Fe (**a**, **c**, **e**) and Mn (**b**, **d**, **f**) for deployments 1 (**a**, **b**), 2 (**c**, **d**) and 3 (**e**, **f**) of the fg-SPI. Solid lines denote profiles obtained from g-SPI gels (black = left, grey = right) and dashed lines denote profiles obtained from SCUBA diver-deployed gel probes ($n = 3$, except $n = 2$ for Fe in deployment 1 and for Mn in deployment 2).
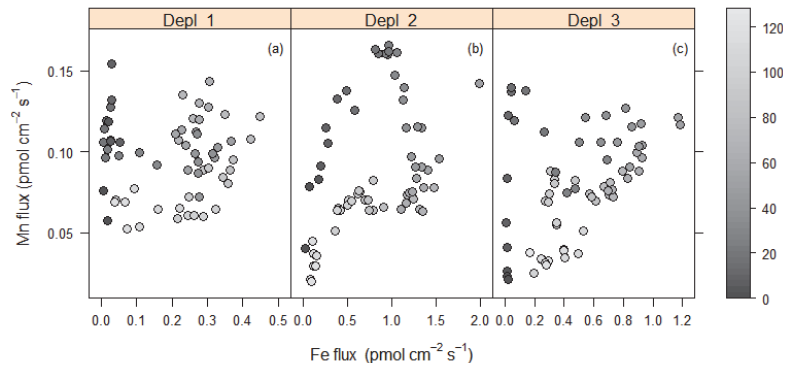
Fig. 4. The relationship between mean Fe ($n = 5$) and mean Mn ($n = 5$) flux with sediment profile depth (mm, indicated by grey shading) from profiles derived during **(a)** deployment 1 **(b)** deployment 2, and **(c)** deployment 3 of the fg-SPI.
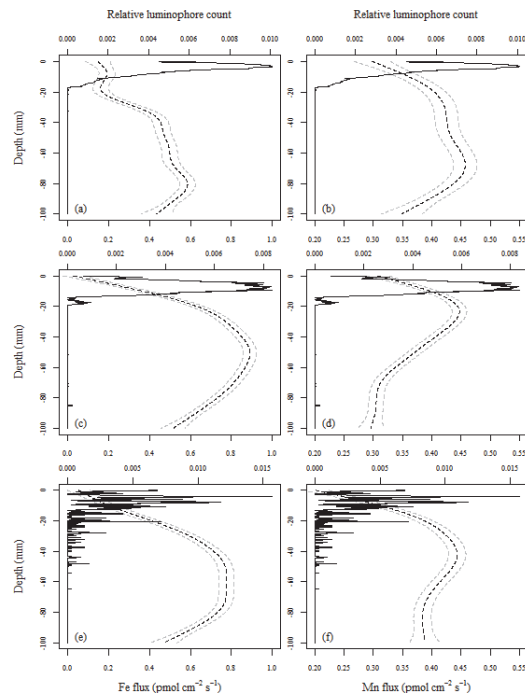
8569

Fig. 5. Predicted trace metal profiles (dotted black lines) ±SE (dotted grey lines) from fitted GAMs for Fe (**a**, **c**, **e**) and Mn (**b**, **d**, **f**) for deployments 1 (**a**, **b**), 2 (**c**, **d**) and 3 (**e**, **f**). Solid black lines show luminophore profiles (relative counts) of the final fg-SPI image from each time-lapse sequence.